A graphical interpretation of the rescaled complementary relationship for evapotranspiration

Richard. D. Crago[1] and Russell J. Qualls[2]

[1] Department of Civil and Environmental Engineering, Bucknell University, Lewisburg, PA, USA

[2] Department of Biological Engineering, University of Idaho, Moscow, ID USA

Key Points:

- The Complementary Relationship (CR) of evaporation can be depicted on graphs of vapor pressure (e) versus temperature (T).
- The CR version proposed by the authors can be expressed in an intuitive and insightful geometric form on an e versus T graph.
- The resulting CR performs well with data from 7 sites in Australia.

Abstract

Wet-surface evaporation equations related to the Penman equation can be represented graphically on vapor pressure (e) versus temperature (T) graphs (Qualls & Crago, 2020). Here, actual regional evaporation is represented graphically on (e, T) graphs using the Complementary Relationship (CR) between actual and apparent potential evaporation. The CR proposed by the authors can be represented in a simple and intuitive geometric form, in which lines representing the regional latent heat flux, LE, and the wet surface (Priestley & Taylor, 1972) evaporation rate, LE_{PT}, intersect at e=0. This approach allows a graphical estimate of LE (or the corresponding mathematical formulation) without the need to know either the wet surface or the apparent potential evaporation rates. The wet surface temperature is needed, and a calculation method for it is provided. The formulation works well using monthly data from seven sites in Australia, even when the same value of the Priestley & Taylor parameter α is used for all sites.

Introduction

A recent summary of methods for potential and actual evaporation rates using standard meteorological data (McMahon, Peel, Lowe, Srikantham, & McVicar, 2013) highlights the Penman (1948), Priestley & Taylor (1972), and Penman-Monteith (Allen, Pereira, Raes, & Smith, 1998) equations, noting that they are ubiquitous in the literature and highly significant for estimating potential (wet surface) or reference crop evaporation. For actual evaporation from watersheds at the monthly timescale using standard meteorological data, McMahon et al. (2013) noted that, "[t]here are a range of techniques available," and then listed the methods developed by Brutsaert & Stricker (1979), Szilagyi & Jozsa (2008), Morton (1983), Morton et al (1985),

Granger (1989), and Granger & Gray (1989). With the possible exception of Granger & Gray (1989), all of these utilized some form of the Complementary Relationship (CR) between actual and potential evaporation, initially proposed by Bouchet (1962). Since that time, there has been a series of developments related to the CR, sparked by the landmark paper by Brutsaert (2015).

The framework of the approach presented here comes from Qualls and Crago (2020; cf. Monteith, 1984; Ma & Szilagyi (2019). Qualls and Crago (2020) developed a graphical interpretation of the Priestley & Taylor (1972) and Penman (1948) equations and explored the theory behind a related wet surface evaporation method that is comparable to the Penman equation, but does not require the well-known assumption regarding the slope of the saturation vapor pressure curve proposed by Penman (1948). While Qualls and Crago (2020) developed concepts related to wet-surface evaporation, the present work applies the same concepts to the CR, making use of recent developments in the CR by Brutsaert (2015), Crago, Szilagyi, Qualls, & Huntington, (2016), Szilagyi, Crago, & Qualls (2016b), Crago & Qualls (2018), and Ma & Szilagy (2019).

In the following sections we will review the framework developed by Qualls and Crago (2020), then apply the same concepts to the CR model by Crago et al. (2016). Then we will apply this method to multiple years of data from seven sites in Australia and discuss the results and implications.

Background

The development and notation in this section closely follow that of Qualls and Crago (2020). The energy budget for land surface evaporation can be written (in W m^{-2}):

$$R_n - G = H + LE \,, \qquad (1)$$

where the left-hand side is the available energy, consisting of net radiation input (R_n) and heat flux into the ground, G, and the right-hand side is the sum of sensible heat flux (H) and latent heat flux LE into the lower atmosphere (Brutsaert W. , 2015). Latent heat flux can be written with a mass transfer equation (Brutsaert, 1982; 2015; Stull, 1988) as:

$$LE = f(u) l_v (e_0 - e_a) , \qquad (2)$$

where l_v is the latent heat of evaporation, e is the water vapor pressure, the subscript 0 indicates a value at the skin of the surface and subscript a indicates a value at measurement height z_a . The wind function, $f(u)$ can be written (Brutsaert, 1982, 2005, 2016) for neutral atmospheric conditions as:

$$f(u) = \frac{0.622 k^2 u}{R_d T_a ln[(z_T - d)/z_{0v}] ln[(z_u - d)/z_0]} , \qquad (3)$$

where k=0.4 is von Karman's constant, u is the wind speed measured at height z_u, R_d is the ideal gas constant for dry air, T_a is the air temperature at z_T, d is the displacement height, z_{0v} is the scalar roughness length for heat and water vapor, and z_0 is the momentum roughness length. The original Penman (1948) wind function of the form $f(u)=c_1+c_2u$, where c_1 and c_2 are constants, could replace (3); all the theoretical developments herein would still be valid.

A heat flux equation analogous to (2) can be written (Brutsaert, 2005) as:

$$H = \frac{p c_p f(u)}{\varepsilon} (T_0 - T_a), \qquad (4)$$

where ρ is the density of air, c_p is the specific heat of air at constant pressure, ε=0.622 is the ratio of the molecular weight of water to that of dry air, and T_0 and T_a are the surface skin and air temperatures, respectively.

Qualls and Crago (2020, c.f. Monteith, 1984) wrote (1) for a saturated surface by expressing *LE* with (2) and *H* with (4), resulting in:

$$l_v f(u)[e^*(T_{0w}) - e_a] + \frac{pc_p f(u)}{\varepsilon}(T_{0w} - T_a) - (R_n - G) = 0, \qquad (5)$$

where T_{0w} is the unknown surface skin temperature that would occur under the prevailing u, T_a, e_a, z_0, z_{0v}, d, and (R_n-G). Note that e_0=e^*(T_{0w}) because the air in contact with the wet surface should be saturated at the wet surface temperature T_{0w}. Saturated vapor pressure e^* can be found from (e.g., Chow , Maidment, & Mays, 1988):

$$e^*(T) = 611\ exp\left(\frac{17.27T}{237.3 + T}\right), \qquad (6)$$

in which the temperature is in Celsius and the vapor pressure is in Pa. After solving (5) with (6) for T_{0w} using a root finder algorithm, the saturated surface latent heat flux can be found from (2) as:

$$LE_{0w} = f(u) l_v [e^*(T_{0w}) - e_a], \qquad (7)$$

where the subscript $_{0w}$ indicates values at the surface with the surface assumed to be saturated.

Szilagyi & Jozsa (2008) proposed a wet surface temperature similar to T_{0w}, and showed that it represents the surface temperature of a small wet patch of ground within a drying region. Szilagyi & Schepers (2014) found experimentally that wet bulb temperatures (a proxy for T_{0w}) taken over a saturated patch remain constant during regional drying, provided the available energy and wind speed remain constant. Szilagyi et al (2016b) suggested that wet patches of any size within a drying region will all have the same value of T_{0w}. Conversely, this means that T_{0w} calculated from (5) under drying actual conditions would be the same as the surface temperature if the entire region was saturated (Szilagyi, Crago, & Qualls, 2016b).

Penman (1948) developed his well-known equation for wet surface evaporation based on (1) (2) and (3), with the addition of the assumption that

$$\frac{e^*(T_{0w}) - e^*(T_a)}{T_{0w} - T_a} = \Delta\,, \qquad (8)$$

where Δ is the slope of the e^* curve (6) at T_a. With this assumption, he found:

$$LE_{pen} = \frac{\Delta}{\Delta + \gamma}(R_n - G) + l_v \frac{\gamma}{\Delta + \gamma} E_A\,, \qquad (9)$$

where

$$E_A = f(u)[e^*(T_a) - e_a], \qquad (10)$$

$\gamma=(c_p)p/(\varepsilon\, l_v)$ is the psychrometric constant, and p is air pressure. Note that, because of (8), (9) does not require a direct estimate of (T_{0w}).

Equation (4) lies, at least implicitly, behind equations (5) and (7)-(10). For (4) to be strictly correct, T_a should be the potential temperature of the air at height z_T, that is, the temperature of a parcel with temperature T_a brought adiabatically down from z_T to the surface. Thus, in (4), (5), and (7)-(10), T_a should be replaced with $T_a+g\cdot z_T/c_p$ (Qualls & Crago, 2020). This correction is minimal for small values of z_T (less than a few meters), but can be significant for measurements above tall forest canopies.

Over a large saturated surface, Slatyer & McIlroy (1961) suggested that E_A should approach zero so that the evaporation rate from (9) approaches the equilibrium evaporation rate:

$$LE_e = \frac{\Delta}{\Delta + \gamma}(R_n - G). \qquad (11)$$

Priestley and Taylor (1972) noted that even very large wet surfaces maintain evaporation rates above LE_e, and suggested that actual LE under "advection free" (more commonly called "minimal advection") conditions is:

$$LE_{PT} = \alpha LE_e \,, \qquad (12)$$

where α is bounded by $1 \leq \alpha \leq (1+\gamma/\Delta)$ based on physical constraints (Priestley & Taylor, 1972).

Equations (9) and (12) can be evaluated over actually saturated surfaces, or for unsaturated surfaces, in which case they are intended to give the apparent evaporation a wet patch would provide in a drying region [in the case of (9)] or the evaporation rate an entire region would have if the region was saturated [in the case of (12)]. This is similar to the interpretation of apparent potential evaporation by Kahler & Brutsaert (2006).

Figure 1 illustrates graphically many of the concepts contained in equations (1)-(12) as well as some in the following section. A brief explanation of Figure 1 follows shortly, but see Qualls & Crago (2020) for more details. The variables included in Figure 1 are further explained in Tables 1 and 2 and the paragraphs following them.

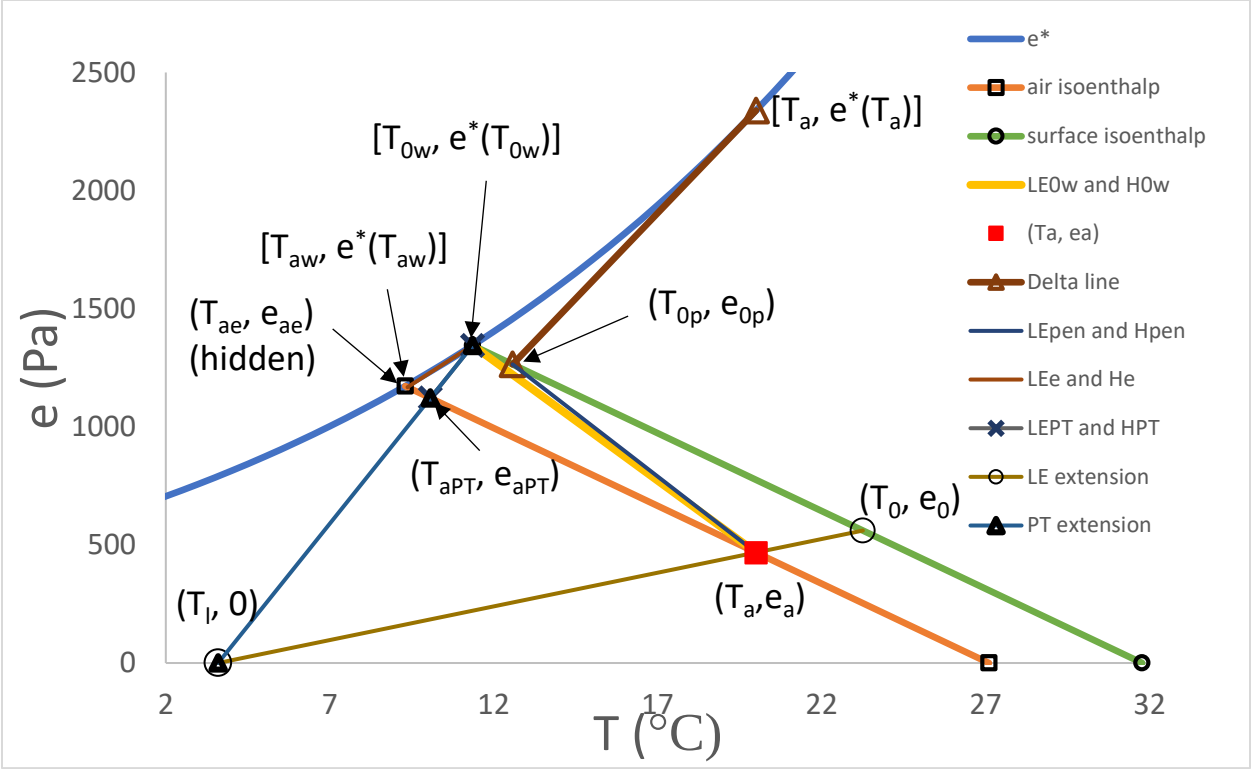

Figure 1. Graphical depiction of evaporation concepts. The graph was developed for the following values: T_a=18°C, relative humidity=0.2, $f(u)$=2.6x10^{-7} s m^{-1}, (R_n-G)=200 W m^{-2}, p=100 kPa, and α=1.26. The labeled points and the lines between them are given in Tables 1 and 2. Adapted from Qualls & Crago (2020).

145 Table 1. Points labeled in Figure 1 [Adapted from Qualls & Crago (2020)]

Point	**Description**
(T_a, e_a)	Measured air T and e
[T_{aw}, $e^*(T_{aw})$]	Intercept of air isoenthalp with e^* curve; T_{aw} = wet bulb air T
[T_{0w}, $e^*(T_{0w})$]	Intercept of surface isoenthalp with e^* curve; T_{0w}=wet surface T
[T_a, $e^*(T_a)$]	Denotes e^* evaluated at T_a;
(T_{0p}, e_{0p})	Intersection between tangent to e^* at T_a and the surface isoenthalp. Used in LE_{pen}
(T_{ae}, e_{ae})	Intersection between tangent to e^* at T_{0w} and the air isoenthalp. Used in LE_e
(T_{aPT}, e_{aPT})	Intersection between line drawn from [T_{0w}, $e^*(T_{0w})$] at slope de/dT=$s\Delta$, where s is from (13), and the air isoenthalp. Used in LE_{PT}
(T_0, e_0)	An estimate of actual skin T and e. Used to find actual LE
(T_l, 0)	Zero-e intercept of line through [T_{0w}, $e^*(T_{0w})$] at slope de/dT=$s\Delta$, where s is from (13). Also intercept of line through (T_0, e_0) and (T_a, e_a)

146

147

Table 2. Lines on Figure 1 [Adapted from Qualls & Crago (2020)].

Line	**Description**
e^*	Saturation vapor pressure curve
Air isoenthalp	Passes through (T_a, e_a) with slope of $-\gamma$
Surface isoenthalp	Located $\varepsilon(R_n\text{-}G)/[p\ c_p\ f(u)]$ to the right, but parallel to, the air isoenthalp
Penman's Δ line	Starts at [T_a, $e^*(T_a)$] with slope tangent to $e^*(T_a)$, intercepting the surface isoenthalp at [T_{0p}, e_{0p}]
LE_{0w}	Connects [T_{0w}, $e^*(T_{0w})$] to (T_a, e_a), so $LE_{0w}=l_v f(u)[e^*(T_{0w})\text{-}e_a]$
LE_{pen}	Connects (T_{0p}, e_{0p}) to (T_a, e_a) so $LE_{pen}=l_v f(u)[e_{0p}\text{-}e_a]$
LE_e	Connects [T_{0w}, $e^*(T_{0w})$] to (e_{ae}, T_{ae}) so $LE_e=l_v f(u)[e^*(T_{0w})\text{-}e_{ae}]$
LE_{PT}	Connects [T_{0w}, $e^*(T_{0w})$] to (e_{aPT}, T_{aPT}) so $LE_{PT}=l_v f(u)([e^*(T_{0w})\text{-}e_{aPT})$
LE_X	Actual regional evaporation from the CR $y=X$, so $LE_X=l_v f(u)(e_0\text{-}e_a)$
LE_{PT} extension	Extends the LE_{PT} line to the zero-e intercept at T_l
LE_X extension	Extends the LE_X line to the zero-e intercept at T_l
LE_{max} *(not shown)*	Vertical distance from $e^*(T_{0w})$ to the e=0 axis

Szilagyi & Jozsa (2008) suggested that Δ in (11) should be evaluated at the air temperature that would prevail if the entire region was saturated. Since H is likely to be small in this context, one might expect this temperature to be similar to T_{0w} (Qualls & Crago, 2020). An alternative definition of LE_e is that it is the minimal evaporation rate possible from a saturated surface at a given available energy (Qualls & Crago, 2020).

This latter concept can be expressed graphically (Figure 1). Qualls & Crago (2020) showed that a line through (T_a, e_a) with slope $de/dT=-\gamma$ is an isobaric line of constant enthalpy. Because this

line passes through (T_a, e_a) it is called the air isoenthalp. This line intersects the e^* curve at the wet bulb air temperature T_{aw}. The surface isoenthalp is a parallel line located a distance $\varepsilon(R_n\text{-}G)$ / $[p{\cdot}c_p{\cdot}\, f(u)]$ to the right of the air isoenthalp, passing through $[T_{0w}, e^*(T_{0w})]$. It represents possible surface skin temperatures and vapor pressures. Straight lines connecting the surface isoenthalp to the air isoenthalp start at points on the surface line (T_0, e_0) and end on the air line (T_a, e_a). Both points can conceivably fall anywhere along their respective isoenthalps, and any two such points automatically produce values of $H{=}p{\cdot}\, c_p{\cdot}f(u)/\varepsilon](T_0\text{-}T_a)$ and of $LE{=}l_v{\cdot}f(u)(e_0\text{-}e_a)$ that satisfy the energy budget (1). Furthermore, since the isoenthalps represent constant enthalpy and we know from (5) that the line from $[T_{0w}, e^*(T_{0w})]$ to (T_a, e_a) produces H and LE values that satisfy (1), it follows that any two points on the surface and air isoenthalps will also satisfy (5). Note that γ depends weakly on temperature, so the isoenthalps are actually not quite straight; however, assuming they are straight is a very good assumption. In fact, when plotted at the scale of Figure 1, any deviation from a straight line is difficult to detect even with a straight edge (Qualls & Crago, 2020).

Minimum wet surface evaporation is represented by a tangent to the e^* curve at T_{0w}, extending to its intercept with the air isoenthalp at point (T_{ae}, e_{ae}), which can be found algebraically using the equations of the two intersecting lines. This latent heat flux is identical to (11) with Δ evaluated at T_{0w}. Minimal advection wet surface evaporation (Priestley & Taylor, 1972) is given by changing the slope of this line (no longer a tangent) through $(T_{0w}, e^*(T_{0w})]$ to $de/dT{=}s\Delta$ (Qualls & Crago, 2020) where:

$$s = \frac{\alpha\gamma}{\Delta(1-\alpha)+\gamma} \quad . \qquad (13)$$

The corresponding latent and sensible heat fluxes LE_{PT} and H_{PT} are defined by (2) and (4), by following the slope de/dT=$s\Delta$ from [T_{0w}, $e^*(T_{0w})$] to the intercept of this line with the surface isoenthalp (see Figure 1) at point (T_{aPT}, e_{aPT}) which can be found algebraically from the equations of these two lines. The formulas for LE_p and LE_{PT} are given in Table 2.

Complementary Relationship

The complementary relationship (Bouchet, 1962) between actual and apparent potential evaporation is predicated on the idea that a drying region will have restricted evaporation which is reflected in overlying air that is drier and warmer than it would be if the regional surface was saturated. Thus, the demand for evaporation can be used to diagnose the rate of regional evaporation. The symmetric Complementary Relationship (CR) for evaporation (e.g., Brutsaert & Stricker, 1979) can be written:

$$LE + LE_p = 2LE_w\,, \qquad (14)$$

where LE is the actual regional evaporation rate, LE_p is the apparent potential evaporation rate, or the latent heat flux from a small saturated patch in the region. The wet surface evaporation rate LE_w is the evaporation rate the region would have, with its given available energy (R_n-G), if (hypothetically) the region was saturated.

In the advection-aridity approach (Brutsaert & Stricker, 1979), LE_p is taken to be LE_{pen} (9) and LE_w is taken to be LE_{PT}. While these definitions have been widely accepted (e.g, Brutsaert, 2015), multiple authors have noted various shortcomings with the symmetric CR (14), including Lhomme & Guillioni (2006), Brutsaert & Parlange (1998), Han & Tian (2017), Pettijohn & Salvucci (2009), Kahler & Brutsaert (2006), and Brutsaert, Cheng, & Zhang (2020). In a highly

202 influential paper, Brutsaert (2015) suggested using $x=LE_w/LE_p$ and $y=LE/LE_p$ to non-
203 dimensionalize the CR. He proposed, on physical grounds, the boundary conditions $y=0$ and
204 $dy/dx=0$ as $x\rightarrow 0$, along with $y=1$ and $dy/dx=1$ as $x\rightarrow 1$, leading to

205 $$y_B = 2x^2 - x^3, \qquad (15)$$

206 as the lowest order polynomial that satisfies the boundary conditions, where the subscript $_B$
207 indicates y as estimated from (15). Equation (15), with LE_p and LE_w defined as described above
208 for the advection-aridity approach, has been used successfully by Brutsaert et al. (2017), Liu et
209 al. (2016), and Zhang et al. (2017).

210 However, Szilagyi et al., (2016a), Crago et al. (2016), and Crago & Qualls (2018) noted a
211 difficulty with the boundary conditions as $x\rightarrow 0$. Specifically, $y\rightarrow 0$ does not imply $x\rightarrow 0$, because
212 LE_p does not reach infinity simply because y→0. Instead, Crago et al. (2016) suggested that
213 $LE_p\rightarrow LE_{pmax}$, where LE_{pmax} can be estimated from (2) [with $e_0=e^*(T_{0w})$ and $e_a=0$]. In this case,
214 the smallest x can get is $x_{min}=LE_w/LE_{max}$, which forms the lower limit for x, at which LE→0.
215 Crago et al (2016) "rescaled" the CR with the transformation

216 $$X = \frac{x - x_{min}}{1 - x_{min}}, \qquad (16)$$

217 and suggested the CR could be written as $y=X$. Thus, "X" will denote a dimensionless latent heat
218 flux estimate found using $y=X$ with (16), and the corresponding estimate of LE will be denoted
219 LE_X. Crago and Qualls (2018) used (16) but calculated E_{pmax} with Penman's Eqn. (9), where the
220 drying power (10) was taken to be $E_A=f(u)[e^*(T_{dry})-0]$, where $T_{dry}=T_a+e_a/\gamma$, and Δ was also
221 estimated at T_{dry}.

222 **Theoretical development**

223 Crago and Qualls (2018) suggested two primary dimensionless variables to characterize the CR.
224 They noted that

225 $$R_e = \frac{LE_w - LE}{LE_w} \qquad (17)$$

226 is a representation of the energy made available when LE decreases below LE_w, and

227 $$R_p = \frac{LE_p - LE_w}{LE_{pmax} - LE_w} \qquad (18)$$

228 is a representation of the energy that must be added to increase LE_p above LE_w. The
229 denominators of both R_e and R_p are the maximum possible values of their respective numerators,
230 Both R_e and R_p reach a value of 0 when the region is saturated, and both reach a value of 1 when
231 the regional surface is desiccated. Thus, it is reasonable to assume that R_e and R_p are the two
232 controlling dimensionless variables in the regional drying process, so the CR can be represented
233 as

234 $$R_e = f(R_p) \qquad (19)$$

235 Each term of equations (17), (18), and (19) can be written by using (2). Specifically, to write
236 LE_p, e_0 is given by $e^*(T_{0w})$ and e_a is the actual vapor pressure of the air. For LE_w, e_0 is written as
237 $e^*(T_{0w})$ and e_a is e_{aPT}. For LE_{pmax}, e_0 is $e^*(T_{0w})$ and e_a=e_l, where e_l is the limiting value of e that
238 would occur if regional evaporation was zero. Substituting into (19) results in

239 $$1 - \frac{LE}{LE_w} = f_1\left(1 - \frac{e_a - e_l}{e_{aPT} - e_l}\right), \qquad (20)$$

240 which implies

241 $$\frac{LE}{LE_w} = f_2\left(\frac{e_a - e_l}{e_{aPT} - e_l}\right), \qquad (21)$$

where f_1 and f_2 are functions to be determined. It is not clear how to estimate e_l, but it is presumably very small so the assumption that e_l=0 appears reasonable. Note that the left-hand side of (21) and the argument of f_2 both go to zero for a regional evaporation rate of zero, and both go to one for a saturated regional surface. These arguments suggest the simple expression:

$$LE = LE_w \frac{e_a}{e_{aPT}} . \qquad (22)$$

Equation (22) could be re-written $y/x=e_a/e_{aPT}$.

Note that X in (16) involves x and x_{min}, which in turn depend on LE_p, LE_w, and LE_{pmax}. Each of these can be expressed using (2) with the appropriate values of e, as described below equation (19). With these substitutions, $y=X$ is easily shown to be identical to (22).

Qualls and Crago (2020) discussed the extension of the LE_{0w} and LE_{pen} lines below and to the left of the air isoenthalp (Figure 1), and noted that this extension corresponds to (T, e) pairs for progressively higher elevations within the constant-flux (surface) layer. With this interpretation, e_l appears to be the vapor pressure at the top of the surface layer or within the mixed layer under very dry surface conditions, such that if $e_0=e_l$, regional evaporation would be zero.

An informative and intuitive geometrical interpretation of $y=X$ or (22) emerges, as shown in Figure 2, which is adapted from Figure 1 by deleting the extraneous information. It can be shown that the extensions of the LE_{PT} line and the LE_X line both reach a vapor pressure of e=0 at the same temperature, T_l. This means that $y=X$ can be expressed graphically on Figure 1 by extending the LE_{PT} line down to the T axis at (T_l, 0), and then drawing a line from (T_l, 0) through (T_a,e_a) to (T_0, e_0). The latent heat flux then is $(l_v)f(u)[e_0-e_a]$. Fluxes from this method are identical to (22) or y=X with X given by (15). Intuitively, looking at the LE_X extension line, an LE_X value of 0 would imply that this line is horizontal, so that (e_0-e_a) is 0, which means this line falls along

the e=0 axis of Figure 1; conversely, maximum regional evaporation would occur if the LE_X line was superimposed on top of the LE_{PT} line. Intermediate values of LE_X would result in the extension lines having intermediate slopes in between these two extremes.

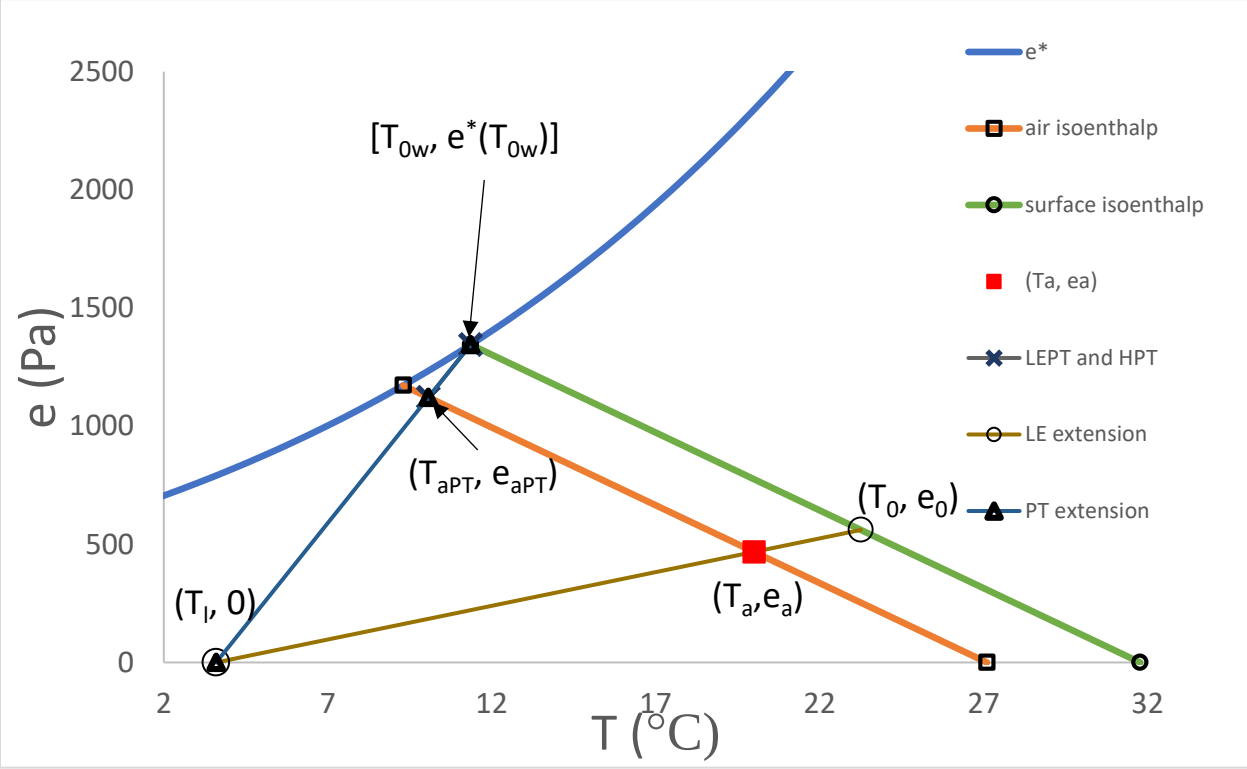

Figure 2. Same as Figure 1, but with extraneous lines and points removed to illustrate the graphical solution to $LE_X=LE_{0w}(e_a/e_{aPT})$.

The simplicity and explanatory power of the $y=X$ assumption follows from this graphical interpretation. Given (R_n-G), $f(u)$, T_a, and e_a, the estimate of LE based on $y=X$ (called LE_X) is easily constructed graphically (see Figure 1):

1. The air isoenthalp passes through (T_a, e_a) at a slope of $de/dT = -\gamma$.
2. The surface isoenthalp is a distance $\varepsilon(R_n\text{-}G)/[p\cdot c_p\cdot f(u)]$ degrees to the right of, and parallel to, the air isoenthalp.

3. The wet surface temperature T_{0w} is given by the intercept of the surface isoenthalp with the e^* curve.
4. Starting at [T_{0w}, $e^*(T_{0w})$], a line having a slope de/dT=$s\Delta$, where s is found using (13) and Δ=de^*/dT evaluated at T_{0w}, is drawn, extending all the way to e=0 at a temperature T_l. [Note that this line intercepts the air isoenthalp at (T_{aPT}, e_{aPT}), but neither the (T, e) values at this point nor the value of LE_{PT} need to be known to complete the graphical construction, only the slope of this line.]
5. A second straight line, starting at the known point (T_l, 0) and passing through (T_a, e_a) is extended to the surface isoenthalp, to the point (T_0, e_0).
6. The actual latent heat flux is calculated as $LE_X=l_v \cdot f(u)(e_0-e_a)$.

When z_T is high enough that T_a differs significantly from the potential temperature of the air, the graphical CR shown in Figure 2 still applies, except the point (T_a, e_a), through which the air isoenthalp passes, should be replaced with [($T_a+g \cdot z_T/c_p$), e_a], as discussed above and by Qualls & Crago (2020).

Note that, while LE_{pa} and either LE_{pmax} or x_{min} play key roles in the derivation of (22), none of them are found in (22), and none are needed to estimate LE using (22). Likewise, none of them need to be known in order to use the graphical method. In actual practice, the calculation of e_{aPT} in (22) is comparable in difficulty to estimating x_{min} and X, so the advantage of (22) is largely conceptual rather than computational. Also, note that LE_{pmax} is proportional to [$e^*(T_{0w})-e_l$], so the concept of LE_{pmax} is incorporated into Figure 2.

In the following section, the y=X using (16) and the y_B= $2x^2$-x^3 (15) versions of the CR will be tested using data from surface flux stations in Australia.

Methods

Data

Data from seven FLUXNET sites in Australia were used, spanning a wide range of environmental conditions, from low crops to tall forests, from arid to humid, and from tropical to temperate climates. This is the same dataset described by Crago & Qualls (2018), except monthly, rather than weekly, data are used here. Longer averaging times are often assumed to satisfy the assumptions behind the CR better (e.g., Szilagyi et al., 2016a; 2016b), and monthly time steps are commonly used in potential evaporation and CR studies (e.g., McMahon et al., 2013).

Each site measured air temperature, vapor pressure, wind speed, net radiation, ground heat flux, and eddy covariance estimates of H, LE, and friction velocity u_*. Monthly average data were downloaded from the Fluxdata web site (http://fluxnet.fluxdata.org/). A summary of the sites is found in Table 3. FLUXNET provides data quality assessment and gap-filling by multiple methods; the method that provided the greatest number of complete months of data was selected. The eddy covariance Bowen ratio was assumed to be correct, and reference (or measured) values of sensible heat flux (H_M) and latent heat flux (LE_M) were found using (1) with this Bowen ratio (see Crago & Qualls, 2018).

Table 3. Description of the sites (adapted from Crago & Qualls, 2018)

Site/Fluxnet ID	Latitude (°S)	Longitude (°E)	IGBP class	z_0 (m)	Tower height (m)	Months of data
Riggs Creek/ AU-Rig	36.65	145.58	Grassland	0.021	2.5	33
Sturt Plain/ AU-Stp	17.15	133.35	Grassland	0.05	4.8	69
Fogg Dam/ (AU-Fog)	12.54	131.31	Permanent wetland	0.15	14.5	30
Ti Tree East/ AU-TTE	22.29	133.64	Open Shrubland	0.28	9.8	15
Howard Springs/ AU-How	12.5	131.15	Woody savanna	2	23	81
Tumbarumba/ AU-Tum	35.66	148.15	Evergreen broadleaf forest	4.6	70	149
Wallaby Creek/ AU-Wac	37.43	145.19	Evergreen broadleaf forest	7.4	110	21

317

318 Data processing

319 At each site, months having negative net radiation, available energy, H_M, or LE_M were rejected,

320 as were months missing any of the data listed above. The roughness length for momentum z_0,

was found using the logarithmic velocity profile equation (e.g., Brutsaert, 2005) and the eddy covariance estimate of u_* for each month. For this calculation, it was assumed that d_0/z_0=4.8, and the scalar roughness length z_{0v} was found with $z_{0v}=z_0/15$ (e.g., Brutsaert W. , 1982; 2005; 2015; Zhang, Cheng, & Brutsaert, 2017). The log-average of the resulting monthly z_0 values was used in (3). Since several of the sites had measurement heights of several tens of meters, all values of T_a were converted to potential temperatures as discussed previously.

Following Crago & Qualls (2018), both dimensionless (X and y_B) and dimensional (LE_X, LE_B) estimates of latent heat flux were compared with measured values (y_M, and LE_M, for dimensionless and dimensional values, respectively). Two separate methods were used to estimate LE_p, LE_w and LE_{pmax}. In the first method, equation (5) was solved for T_{0w}, then LE_{0w} [estimated from (7)] was used for LE_p, and LE_{pmax} was found with (2) where $e_0=e^*(T_{0w})$ and $e_a=e_l=0$. Wet surface evaporation rate LE_w was found using the equation for LE_{PT} from Table 2; this is equivalent to (12) with (11), where Δ is evaluated at T_{0w}. The resulting LE_p, LE_w and LE_{max} were used with (15) and (16) to estimate latent heat fluxes. We denote these estimates of dimensionless fluxes as X_{0w} and y_{B0w}, and evaluate them by comparing them to reference values $y_M = LE_M/LE_{0w}$, and we will denote the dimensional fluxes as LE_{X0w} and LE_{B0w} and compare them to reference (measured) values LE_M.

The second method used circumvents the primary disadvantage of LE_{0w} compared to LE_{pen}, that LE_{0w} requires a root finder to determine T_{0w}. Specifically, LE_p was estimated with LE_{pen} from (9), where Δ was evaluated at T_a. Wet surface evaporation LE_w was found using (12) with (11), where Δ was estimated at T_a [rather than at T_{0w} as for LE_{PT} (see Table 2)]. For LE_{max}, (9) with (10) was used, where Δ was estimated at T_{dry}, E_A was taken as $f(u)[e^*(T_{dry})-0]$, and $T_{dry}=T_a+e_a/\gamma$ is the e=0

intercept of the air isoenthalp (Crago & Qualls, 2018). We denote these estimates of dimensionless fluxes as X_{pen} and y_{Bpen}, and evaluate them by comparing them to reference values $y_{Mpen} = LE_M/LE_{pen}$, and we will denote the dimensional fluxes as LE_{Xpen} and LE_{Bpen} and compare them to reference values LE_M.

For each of these latent heat flux variables, the root mean square difference (RMSD), or the square root of the mean of the square of the difference between the estimate and the reference values, was calculated. The RMSD was calculated for a range of values of α. The calibrated value of α is that which minimizes RMSD of the chosen variable (y_M, X, LE_X, or LE_B). A different value of α was found for each of the eight estimates (X, y_B, LE_X, LE_B, each using both the LE_{0w} and the LE_{pen} method), but in each estimate, the same value of α was applied to all seven sites.

Results

Results are shown in Figures 3 through 6 and in Table 4. Table 5 provides results when it is assumed that α=1.26 for all sites and methods. In Tables 4 and 5, R is the coefficient of correlation, and "Slope / Int" gives the linear regression slope and intercept between the model estimates and reference values in the form: reference_value = *Slope* * model_value + *Int*. Notice that dimensionless y_M values using LE_{0w} are different than those using LE_{pen}, because different estimates of apparent potential evaporation are used; this is not the case for dimensional estimates.

The application of the same value of α to each of the sites differs from the approach used by Crago and Qualls (2018), but fits with the approach of Priestley & Taylor (1972), who attempted

365 to find a single value appropriate to a number of sites under conditions of minimal advection
366 over a wet surface. This will be discussed more in the discussion section.

367

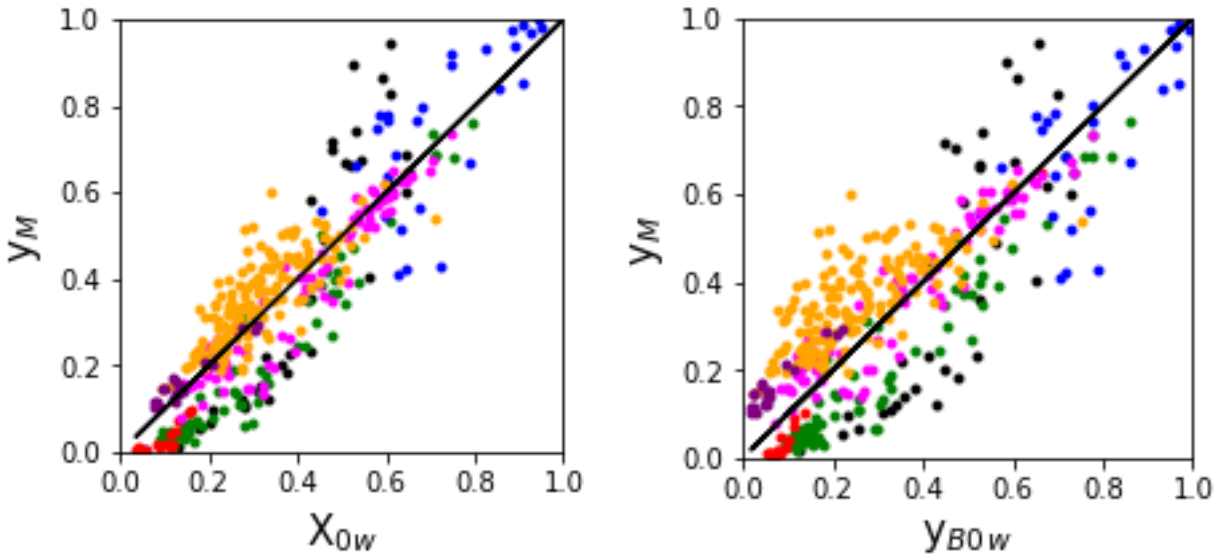

368

369 Figure 3. Results for the dimensionless latent heat flux estimates using the LE_{0w} method. The left
370 panel plots X_{0w} against y_M, and the right plots y_{B0w} against y_M. Dot colors (color / site): (Black /
371 Riggs Creek); (Green / Sturt Plain); (Blue / Fogg Dam); (Red / Ti Tree East); (Magenta--
372 Howard Springs); (Orange—Tumbarumba); (Purple--Wallaby Creek). The black line is one-to-
373 one.

374

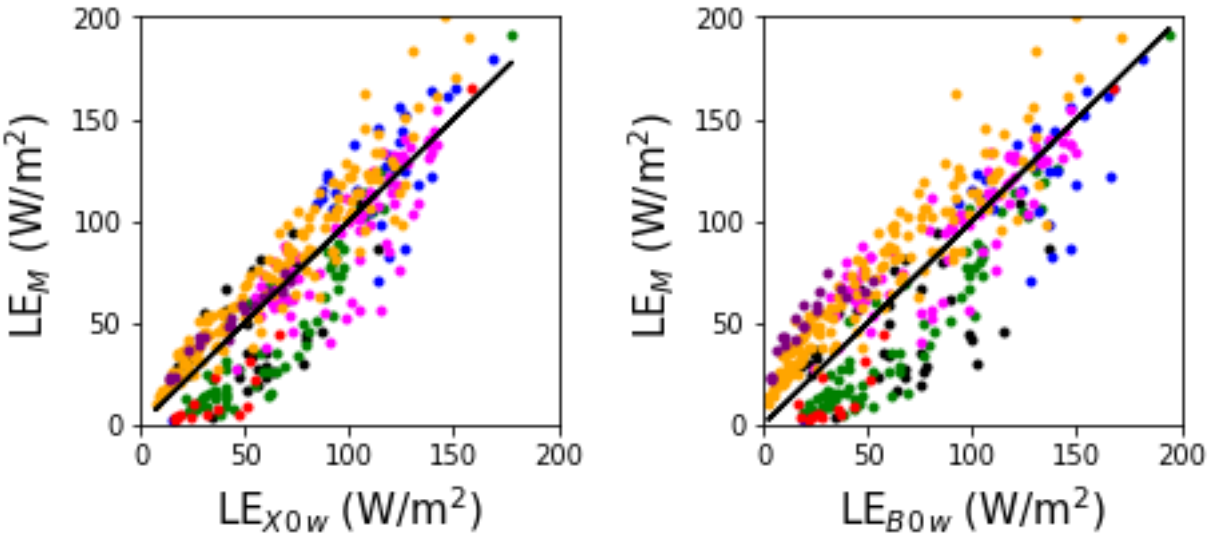

Figure 4. Same as Figure 2, except for dimensional latent heat fluxes. Both panels have one data point outside the range of the graph: in the left panel at (153, 212) W m^{-2}; in the right panel at (167, 212) W m^{-2}.

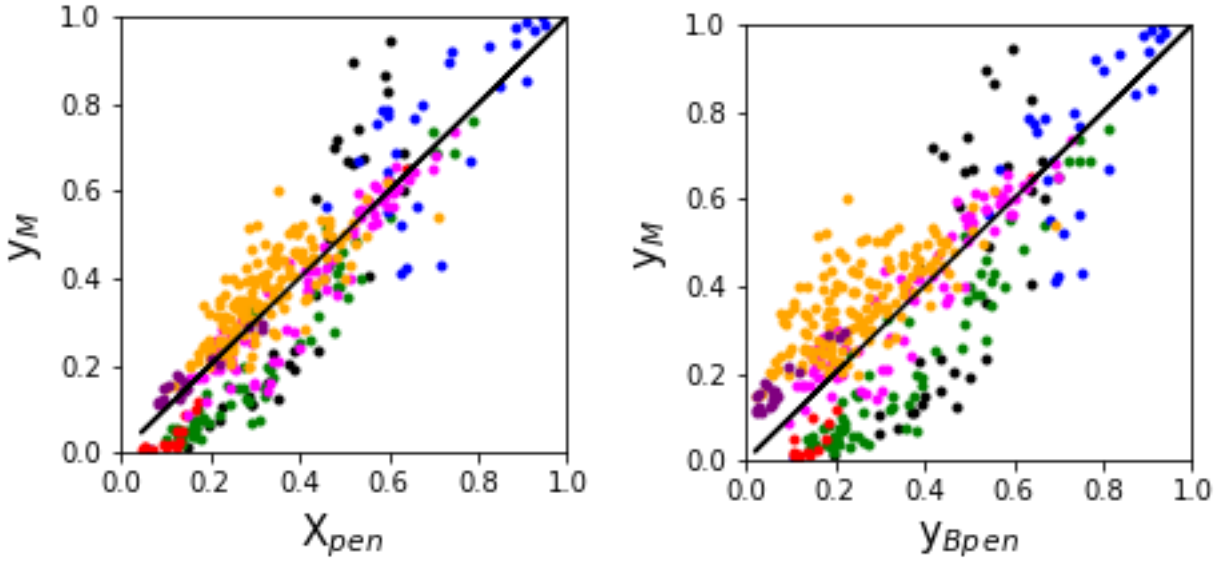

Figure 5. Same as Figure 2 except using the LE_{pen} method.

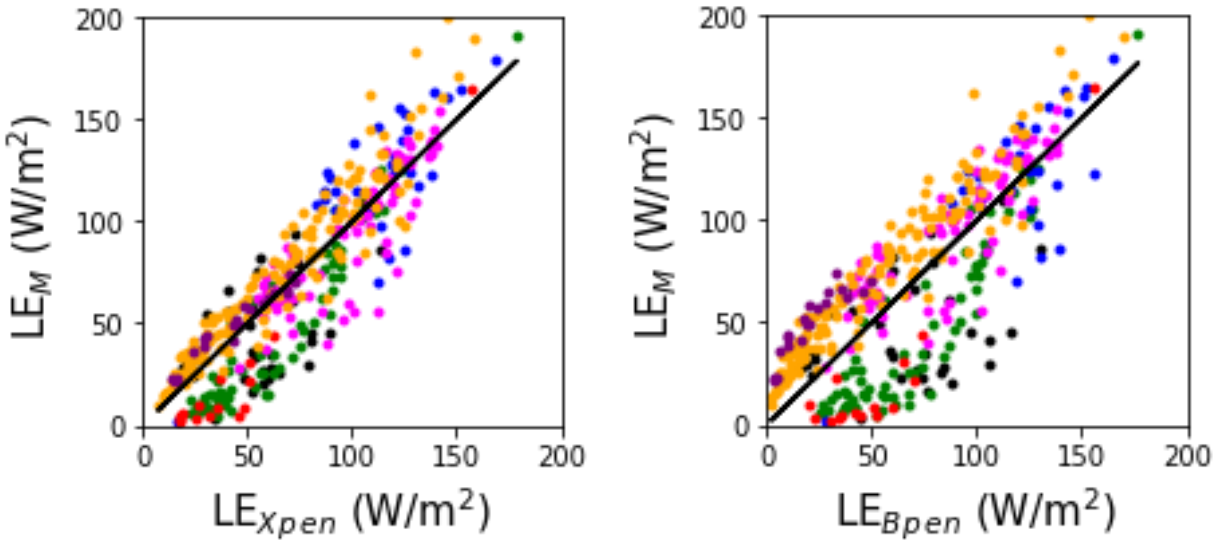

Figure 6. Same as Figure 3 except using the LE_{pen} method. Both panels have one data point outside the range of the graph: in the left panel at (153, 212) W m^{-2}; in the right panel at (175, 212) W m^{-2}.

388 Table 4. Summary of results

	X_{0w}	y_{B0w}	X_{pen}	y_{Bpen}
α	1.18	1.24	1.20	1.17
RMSD	0.097	0.124	0.097	0.137
R	0.90	0.86	0.90	0.80
[1]**Slope/Int**	1.05 / -0.02	0.84 / 0.07	1.07 / -0.03	0.859/0.06
	LE_{X0w}	LE_{B0w}	LE_{Xpen}	LE_{Bpen}
α	1.14	1.23	1.17	1.14
RMSD (W m^{-2})	19.7	24.3	19.1	26.1
R	0.90	0.85	0.90	0.82
[1]**Slope/Int (W m^{-2})**	1.05 / -4.2	0.86 / 12.3	1.06 / -5.5	0.89 / 10.2

389 [1] Linear regression constants: reference = slope*estimate + Int

390 Table 5. Summary of results with α=1.26

	X_{0w}	y_{B0w}	X_{pen}	y_{Bpen}
α	1.26	1.26	1.26	1.26
RMSD	0.102	0.124	0.101	0.145
R	0.9	0.86	0.90	0.8
[1]**Slope/Int**	0.96 / -0.02	0.82 / 0.07	0.99 / -0.02	0.78 / 0.06
	LE_{X0w}	LE_{B0w}	LE_{Xpen}	LE_{Bpen}
α	1.26	1.26	1.26	1.26
RMSD (W m^{-2})	22.2	24.6	20.8	29.2
R	0.9	0.85	0.90	0.82
[1]**Slope/Int (W m^{-2})**	0.92 / -3.7	0.83 / 11.9	0.96 / -4.7	0.78 / 9.1

391 [1] Linear regression constants: reference = slope*estimate + Int

392

393 **Discussion**

394 *Comparison of the generalized and the rescaled versions of the CR*

395 A comparison of the statistics for the models involving X with the corresponding models
396 involving y_B in Table 4 shows that the rescaled versions (those with X and LE_X in the column
397 heading) perform better than the generalized form (y_B and LE_B) when a single value of α is used
398 for all the sites. Even when the values of α that provide the optimal results for LE_B and y_B are

used to estimate LE_X and X, the latter give smaller RMSD and larger R values than the former (results not shown). Table 5 shows that (16) also gives smaller RMSD and larger R than (15) when a value of α=1.26 (Priestley & Taylor, 1972) is assumed for all sites and methods.

This strong performance by versions of the rescaled CR fits with the findings of Crago and Qualls (2018) using the same dataset (but the current study uses monthly rather than weekly values). Those earlier results allowed for the calibration of site-specific values of α, and the improvement of the rescaled CR (16) over the generalized (15) was less conclusive than the present findings. Apparently, the generalized model benefitted from the use of calibrated, site-specific values of α (in Crago and Qualls, 2018) more than the rescaled model did, so that when the data from all sites were pooled and a single value of α was used for all sites, performance of the generalized model decreased more than that of the rescaled model.

Use of LE_{pen} instead of LE_{0w}

Tables 4 and 5 also compare CR versions based on the LE_{0w} method with those based on the LE_{pen} method (both described above). For the generalized model (15), the LE_{0w} method gives somewhat better results than the LE_{pen} method (for example, y_{B0w} does better than y_{Bpen} in terms of lower RMSD combined with higher values of R). However, for the rescaled model (versions labeled X_{0W}, X_{pen}, LE_{X0w}, and LE_{Xpen} in Tables 4 and 5), the formulations using LE_{pen} and LE_{0w} have comparable performances, although LE_{Xpen} has a somewhat smaller (better) RMSD than the LE_{X0w} version does.

On the other hand, as shown by Qualls & Crago (2020), and in the theory section of this paper, LE_{0w} has clear theoretical advantages over LE_{pen}, and it leads to fruitful and informative theoretical developments, such as the derivation of (22) and the graphical interpretation of the

CR shown in Figure 2. On these grounds the LE_{0w} method is preferable. Actually, a comparison of the columns in Tables 4 and 5 suggests that the use of either of the two versions of the rescaled CR model is more important than the exact formulation of that model, and a case could be made for either the LE_{pen} or the LE_{0w} method. However, for the remainder of the Discussion section, we will focus mainly on the LE_{0w} method and its graphical interpretation.

Discussion of the graphical construction of the CR

If we assume that R_n-G and $f(u)$ are held constant as a region dries (c.f., Brutsaert, 2015), T_{0w} should also remain constant (Szilagyi & Schepers, 2014), so the regional drying process results in sliding of the point (T_a, e_a) down and to the right along the air isoenthalp. The value of LE_w=LE_{PT} should remain constant since T_{0w} is constant during dry-down. This means that the e=0 intercept of the Priestley-Taylor line at (T_l, 0) should remain constant as well. Thus, the drying process is reflected by a clockwise rotation or slowly decreasing slope of the line from (T_l, 0) to (T_a, e_a) as the latter point slides down the air isoenthalp during regional drying (Figure 2). This results in a corresponding decrease in (e_0-e_a) and thus in a decrease of LE.

The role of α in the production of actual regional LE values, and how this impacts the graphical CR construction, deserves some discussion here. The value of α has been studied extensively (e.g., Brutsaert, W., 1982; 2005; Lhomme & Guilioni, 2010; McNaughton & Spriggs, 1989; Priestley & Taylor, 1972). For very large wet surfaces with minimal advection, Priestley & Taylor (1972) originally estimated α = 1.26. For truly wet surfaces with minimal advection, most estimates fall in the range $1.20 \leq \alpha \leq 1.30$ (Brutsaert, 2005).

Bouchet's (1962) CR concept requires that a relatively large regional LE should result in relatively high moisture content in the atmospheric boundary layer (ABL). Conversely, a

relatively dry ABL implies a relatively small regional *LE*. Having a value of α>1 modifies this process, because α>1 represents the import of dry air from outside the regional ABL, largely through the entrainment of free atmosphere air. This prevents the ABL from reaching full equilibrium with the moisture status of the surface skin (e.g., Lhomme & Guilioni, 2006; 2010; McNaughton & Spriggs, 1989; Raupach, 2001).

Larger values of α mean more incorporation of dry air into the ABL, such that the humidity of the ABL is lower for a given *LE* than it would be at equilibrium (α=1). This examination of the physical process suggests that, for given values of T_a, (R_n-G), and $f(u)$, values of α>1 should correspond to greater entrainment of dry air and thus lower e_a for a given value of *LE* than if α was equal to 1. Increasing the value of α reduces the anticipated value of e_a. Alternatively, if all else is equal, a given (T_a, e_a) would be expected to result from a larger *LE,* if α is larger.

A properly formulated CR should reflect this. According to the graphical CR model illustrated in Figure 2, T_{0w} and α together determine the slope of the line from [T_{0w}, $e^*(T_{0w})$] to (T_l, 0). The point (T_0, e_0) lies at the intersection of the surface isoenthalp with the line that passes from (T_l, 0) through (T_a, e_a) (see Figure 2). With this graphical interpretation, a larger α corresponds to a steeper slope (larger de/dT) of the line through [T_{0w}, $e^*(T_{0w})$] and (T_{aPT}, e_{aPT}), and thus to a larger T_l. This in turn gives a steeper LE_X line and a larger value for (e_0-e_a) and a larger regional *LE* because of (2). The dynamic illustrated in Figure 2 thus fits our understanding of how ABL dynamics impact α and regional *LE*.

While it is not uncommon to treat α as a local or regional variable to be determined by calibration (Brutsaert et al., 2017; Crago et al., 2016; Crago & Qualls, 2018; Zhang et al., 2017), Priestley & Taylor (1972) treated local values of α as instances of a more universal constant, arriving at the well-known value α=1.26 through averaging the local estimates. The relatively

narrow range (Brutsaert, 2005) of estimates noted above seems to support this. Conversely, Brutsaert (2005) also discusses the inherent inhomogeneity and unsteadiness of actual atmospheric boundary layer (ABL) processes, which seem likely to result in some variability in α.

It would appear that different free atmospheric conditions and ABL growth rates might result in different values of α. There is a long history of treating α as a constant with a value in the vicinity of 1.26, both in studies of wet-surface evaporation (Priestley & Taylor, 1972; Brutsaert, 2005; Eichinger, Parlange, & Stricker, 1996), and in studies of the CR (e.g., Brutsaert & Stricker, 1979; Szilagyi, 2015; 2018; Szilagyi et al., 2016). At the same time, other studies suggest that it is not constant (e.g., Lhomme J. -P., 1997; Pereira, 2004; Viswanadham et al., 1991) or needs to be locally calibrated (e.g., Ma, et al., 2015). McMahon et al. (2013) provide a relatively recent review of the literature.

While some of this evidence points to the advantages of local calibration of α, the need for local calibration severely limits the applicability of the CR, particularly in data-scarce regions. This consideration supports the use of a single constant value of α, provided reasonable results come from it, as they do here. Note that, although the optimal values of α found for the rescaled model in this study were slightly below the typical range ($1.20 \leq \alpha \leq 1.30$) found by Brutsaert (2005), the present estimates are comparable to the values of 1.13 (Szilagyi et al., 2016b) and 1.15 (Szilagyi, 2018) obtained from long-term (1979-2015) reanalysis data from the wettest of the 334 Hydrologic Unit Code level-6 watersheds in the contiguous United States; these latter estimates were independent of the CR.

Looking at the two lines passing through (T_l, 0) in Figure 1, it is clear that changing the value of α and thus of T_l will have a larger impact when LE is very close to LE_{PT}, than when LE is very

close to zero, because the slope of the line connecting (T_l, 0) to (T_0, e_0) is relatively sensitive to T_l when the regional air is very moist, and not as sensitive when the regional air is relatively dry (far down and to the right on the air isoenthalp). In the limit as $e_a \rightarrow 0$, T_l has no impact on LE.

Note that the graphical interpretation of the CR could also incorporate a non-zero value for e_l, the minimal value of e corresponding to a regional value of LE=0. In this case, T_l would be the intercept of the LE_{PT} line with a horizontal line at e=e_l. Then the line through (T_l, e_l) and (T_a, e_a) would intersect the surface isoenthalp at (T_0, e_0) and (e_0-e_a) in (2) would give the regional LE.

As shown in Table 5, model performance degrades slightly when α=1.26 is used rather than the value that minimizes RMSD. The rescaled CR model still outperforms the generalized CR model in both R and RMSD.

Conclusions

The CR is emerging as an essential conceptual tool for researchers seeking to estimate evaporation from a region (McMahon et al., 2013). Beginning with the concepts of potential and apparent potential evaporation, the CR compares these two versions of wet surface evaporation and infers a regional actual evaporation rate. In this study, theoretical considerations and their graphical representation suggested by Qualls & Crago (2020) are applied to evaluate the rescaled CR (Crago et al., 2016; Szilagyi et al., 2016, Crago & Qualls, 2018, Ma N. , Szilagyi, Zhang, & Liu, 2019, Ma & Szilagyi, 2019). By writing potential and apparent potential evaporation in the form of mass transfer equations involving the vapor pressure at the surface skin and aloft in the surface layer, this study shows that the rescaled CR formulation y=X can be expressed through lines and points on a graph of vapor pressure versus temperature. A purely graphical version of the CR, along with its mathematical expression, is described. This rescaled CR is shown to

provide estimates of regional dimensional and dimensionless evaporation rates better than those provided by the generalized CR (15) for seven flux stations in Australia.

Crago and Qualls (2013), discussed the contributions of Wilfried Brutsaert to intuitive or conceptual models in hydrology, in particular to the CR and to the conservation of evaporative fraction during the daytime. They pointed out that intuitive concepts allow investigators to see or grasp a topic in a new and profound way, without necessarily requiring a comprehensive understanding of all the underlying physical processes. We hope the graphical approach taken here and in Qualls and Crago (2020) will help researchers gain an intuitive grasp of wet surface evaporation and of the CR, and by means of that insight to further improve our collective understanding of the evaporation process.

Acknowledgements:

The data used in this paper came from the FLUXNET project and were obtained through the Fluxdata web site (https://fluxnet.fluxdata.org/).

References

Allen, R. G., Pereira, L. S., Raes, D., & Smith, M. (1998). *Crop Evapotranspiration--Guidelines for Computing Crop Water Requirements--FAO Irrigation and Drainage Paper 56.* Rome: Food and Agriculture Organization of the United Nations.

Blaney, H. F., & Criddle, W. D. (1962). *Determining Consumptive Use and Irrigation Water Requirements, Technical Bulletin 1275.* Washington, D.C.: Agricultural Research Servicie, United States Departement of Agriculture.

532 Bouchet, R. J. (1962). Evapotranspiration reelle et potentielle, signification climatique. *Int. Assoc. Sci.*
533 *Hydrol. Publ. 62*, 134-142.

534 Brutsaert, W. (1982). *Evaporation into the Atmosphere: Theory, History, and Applications.* Dordrecht,
535 Holland: D. Reidel .

536 Brutsaert, W. (2005). *Hydrology, An Introduction.* New York, NY: Cambridge University Press.

537 Brutsaert, W. (2015). A generalized complementary principle with physical constraints for land-surface
538 evaporation. *Water Resources Research, 51*(10), 8087-8093.
539 https://doi.org/10.1002/2015WR017720.

540 Brutsaert, W., & Parlange, M. B. (1998). Hydrologic cycle explains the evaporation paradox. *Nature*,
541 6706.

542 Brutsaert, W., & Stricker, H. (1979). An advection-aridity approach to estimate actual regional
543 evapotranspiration. *Water Resources Research (15)*, 443-449.
544 https://doi.org/10.1029/WR015i002p00443.

545 Brutsaert, W., Takahashi, A., Hiyama, T., Zhang, L., & Liu, W. (2017). Nonlinear advection-aridity method
546 for landscape evaporation and its application during the growing season in the southern Loess
547 Plateau of the Yellow River basin. *Water Resources Research (53)*, 270-282.

548 Bureau of Meteorology, G. o. (n.d.). *Water and Land for Agriculture and Natural Resources*
549 *Management*. Retrieved Apr 6, 2019, from
550 http://www.bom.gov.au/watl/eto/tables/nt/darwin_airport/darwin_airport.shtml

551 Chow , V. T., Maidment, D. R., & Mays, L. M. (1988). *Applied Hydrology.* New York: McGraw-Hill.

552 Crago, R., & Qualls, R. J. (2018). Evaluation of the generalized and rescaled complementary evaporation
553 relationships. *Water Resources Research, 54*(doi10.1029/2018WR023401), 8086-8102.
554 https://doi.org/10.1029/2018WR023401.

555 Crago, R., Szilagyi, R., Qualls, R., & Huntington, J. (2016). Rescaling the complementary relationship for
556 land surface evaporation. *Water Resources Research, 52*, 8461-8471.
557 https://doi.org/10.1002/2016WR019753.

558 Eichinger, W. E., Parlange, M. B., & Stricker, H. (1996). On the concept of equilibrium evaporation and
559 the value of the Priestley-Taylor coefficient. *Water Resources Research*, 161-164.
560 https://doi.org/10.1029/95WR02920.

561 FLUXNET. (2014, 11 6). *Fluxdata: the data portal serving the FLUXNET community*. Retrieved Apr 6, 2019,
562 from https://fluxnet.fluxdata.org/community/highlights/

563 Granger, R. J. (1989a). A complementary relationship approach for evaporation from nonsaturated
564 surfaces. *Journal of Hydrology*, 31-38. https://doi.org/10.1016/0022-1694(89)90250-3.

565 Granger, R. J., & Gray, D. M. (1989b). Evaporation from natural nonsaturated surfaces. *Journal of*
566 *Hydrology, 111*, 21-29.

567 Han, S., & Tian, F. (2017). Derivation of a sigmoid generalized complementary function for evaporatio
568 with physical constraints. *Water Resources Research, 54*(7), 5050-5068.

569 Hobbins, M. T., Ramirez, J. A., & Brown, T. C. (2004). Trends in pan evaporation and actual
570 evapotranspiration across the conterminous US: Paradoxical or complementary? *Geophysical*
571 *Research Letters*, 31 (13).

572 Kahler, D. M., & Brutsaert, W. (2006). Complementary relationship between daily evaporation in the
573 environment and pan evaporation. *Water Resources Research, 42*, doi:10.1029/2005WR004541.

574 Lhomme, J. -P. (1997). A theoretical basis for the Priestley-Taylor coefficient. *Boundary-Layer*
575 *Meteorology, 82*, 179-191.

576 Lhomme, J. P., & Guilioni, L. (2010). On the link between potential evaporation and regional evaporation
577 from a CBL perspective. *Theoretical and Applied Climatology, 101(1-2)*, 143-147.

578 Lhomme, J. P., & Guillioni, L. (2006). Comments on some articles about the complementary relationship.
579 *Journal of Hydrology (323)*, 1-3.

580 Liu, X., Liu, C., & Brutsaert, W. (2016). Regional evaporation estimates in the eastern monsoon region of
581 China: Assessment of a nonlinear formulation of the complementary principle. *Water Resources*
582 *Research*, 9511-9521.

583 Ma, N., Zhang, Y., Szilagyi, J., Guo, Y., Zhai, J., & Gao, H. (2015). Evaluating the complementary
584 relationship of evapotranspiration in the alpine steppe of the Tibetan Plateau. *Water Resources*
585 *Research, 51*, 1069-1083.

586 McMahon, T. A., Peel, M. C., Lowe, L., Srikantham, R., & McVicar, T. R. (2013). Estimating actual,
587 potential, reference crop and pan evaporation using standard meteorological data: a pragmatic
588 synthesis. *Hydrology and Earth System Sciences*, 1331-1363, doi:10.5194/hess-17-1331-2013.

589 McNaughton, K. G., & Black, T. A. (1973). A study of evapotranspiration from a Douglas fir forest using
590 the energy balance approach. *Water Resources Research (9)*, 1579-1590.

591 McNaughton, K. G., & Spriggs, T. W. (1989). An evaluation of the Priestley and Taylor equation and the
592 complementary relationship using results from a mixed-layer model of the convective boundary
593 layer. *Estimation of Areal Evapotranspiration, IAHS Publ. no. 177* (pp. 89-104). Vancouver: IAHS.

594 Monteith, J. L., & Unsworth, M. (2001). *Principles of Environmental Physics, 2nd Edition.* Oxford:
595 Butterworth-Heinemann.

596 Morton, F. I. (1983). Operational estimates of areal evapotranspiration and their significance to the
597 science and practice of hydrology. *Journal of Hydrology, 66*, 1-76.

598 Morton, F. I., Richard, F., & Fogarasi, S. (1985). *Operational estimates of areal evapotranspiration and*
599 *lake evaporation--Program WRE-VAP, NHRI Paper 24.* Ottawa: Inland Waters Directorate,
600 Environment Canada.

601 Penman, H. L. (1948). Natural evaporation from open water, bare soil and grass. *Proc. Roy. Soc. London,*
602 *A 193, 193*(1032), 120-145.

603 Pereira, A. R. (2004). The Priestley-Taylor parameter and the decoupling factor for estimating reference
604 crop evapotranspiration. *Agricultural and Forest Meteorology, 125*, 305-313.

605 Pettijohn, J. C., & Salvucci, G. D. (2009). A new two-dimensional physical basis for the complementary
606 relationship between terrestrial and pan evaporation. *Journal of Hydrometeorology, 10*, 565-
607 574. https://doi.org/10.1175/2008JHM1026.1.

608 Priestley, C. H., & Taylor, R. J. (1972). On the assessment of surface heat flux and evaporation using
609 large-scale parameters. *Monthly Weather Review, 100*, 81-92.

610 Qualls, R. J., & Crago, R. (2020). Graphical Interpretation of Wet Surface Evaporation Equations. *In*
611 *review*.

612 Raupach, M. R. (2001). Combination theory and equilibrium evaporation. *Quarterly Journal of the Royal*
613 *Meteorological Society, 127*, 1149-1181.

614 Slatyer, R. O., & McIlroy, I. C. (1961). *Practical Microclimatology.* Melbourne, Australia: CSIRO.

615 Stull , R. B. (1988). *An Introduction to Boundary Layer Meteorology.* Norwell, MA: Kluwer Academic
616 Publishers.

617 Szilagyi, J. (2015). Complementary-relationship-based 30 year normals (1981-2010) of monthly latent
618 heat fluxes across the contiguous United States. *Water Resources Research, 51*,
619 doi:10.1002/2015WR017693.

620 Szilagyi, J. (2018). A calibration-free, robust estimation of monthly land surface evapotranspiration rates
621 for continental-scale hydrology. *Hydrology Research, 49(3)*, 648-657.

622 Szilagyi, J. (2018). Anthropogenic hydrological cycle disturbance at a regional scale: State-wide
623 evapotranspiration trends (1979-2015) across Nebraska, USA. *Journal of Hydrology, 557*, 600-
624 612.

625 Szilagyi, J., & Jozsa, J. (2008). New findings about the complementary relationship-based evaporation
626 estimation methods. *Journal of Hydrology*, 171-186.

627 Szilagyi, J., & Schepers, A. (2014). Coupled heat and vapor transport: The thermostat effect of a freely
628 evaporating land surface. *Geophysical Research Letters*, 435-441.

629 Szilagyi, J., Crago, R., & Qualls, R. (2016). A calibration-free formulation of the complementary
630 relationship of evaporation for continental-scale hydrology. *J. Geophys. Research: Atmos.*, 264-
631 278.

632 Szilagyi, J., Crago, R., & Qualls, R. J. (2016). Testing the gneralized complementary relationship of
633 evaporation with continental-scale long-term water-balance data. *J. Hydrology, 540*, 914-922.

634 Viswanadham, Y., Silva Filho, V. P., & Andre, R. G. (1991). The Priestley-Taylor parameter α for the
635 Amazon forest. *Forest Ecology and Management, 38*, 211-225.

636 Zhang, L., Cheng, L., & Brutsaert, W. (2017). Estimation of land surface evaporation using a generalized
637 nonlinear complementary relationship. *Journal of Geophysical Research: Atmospheres*, 1475-
638 1487.

639